Int. J. Bio-Inorg. Hybd. Nanomat., Vol. 1, No. 3 (2012), 137-149

International Journal of Bio-Inorganic Hybrid Nanomaterials

Hydrothermal Synthesis, Characterization, Optical Properties of Lithium Meta- and Disilicate Nanomaterials and Theoretical Calculations

Abdolali Alemi[1]*, Shahin Khademinia[1], Sang Woo Joo[2], Mahboubeh Dolatyari[3], Akbar Bakhtiari[3]

[1] Department of Inorganic Chemistry, Faculty of Chemistry, University of Tabriz, Tabriz, Iran
[2] School of Mechanical Engineering, WCU Nano Research Center, Yeungnam University, Gyongsan 712-749 South Korea
[3] Laboratory of Photonics & Nano Crystals, School of Engineering-Emerging Technologies, University of Tabriz, Tabriz, Iran

Received: 20 June 2012; Accepted: 24 August 2012

ABSTRACT

Highly crystalline and pure lithium metasilicate (Li_2SiO_3) and lithium disilicate (Li_2Si2O_5) nanomaterials were synthesized by hydrothermal method and characterized by PXRD technique. The changes in the morphology and particle size of the synthesized nanomaterials with reaction time were investigated using SEM technique. The UV-Vis and photoluminescence spectra of the compounds were studied. The intensity of the bands in the emission spectra increased with increasing reaction time in both compounds. The electronic band structure along with density of states (DOS) calculated by the DFT method that indicated Li_2SiO_3 and $Li_2Si_2O_5$ had an indirect energy band gap of 4.575 eV and 4.776 eV, respectively. The optical properties, including the dielectric, absorption, reflectivity and energy-loss spectra of the compounds were calculated by DFT method and analyzed based on the electronic structures.

Keyword: Hydrothermal method; Lithium silicates; Nanomaterials; Optical properties; DFT calculations.

1. INTRODUCTION

Silicates are the most abundant and most complicated class of minerals on earth that have tremendous technological applications in such fields as catalysis, microelectronics, biomedicine, photonics, and traditional glass and ceramic industries [1]. In particular, the crystalline lithium

(*) Corresponding Author - e-mail: : alemi@tabrizu.ac.ir

silicates are present as important phases in silicate glass ceramics [2]. They are of research interest because of their technological applications in areas such as CO_2 was captured [3-6], lithium battery cathode materials [7], fast ion conductors [8], optical wave-guides [9] and tritium breeding materials [10, 11].

Synthesis of lithium silicates has been performed using different methods, such as solid state reaction [7], precipitation, sol-gel method [9, 13], extrusion-spherodisation process [12, 14], rotating melting procedures [15], combustion [16], electrochemical method [16] and recently via hydrothermal method in different condition and synthesized materials morphologies [16]. However, most of the time, a mixture of Li_2SiO_3, $Li_2Si_2O_5$, Li_4SiO_4 [7, 9] and SiO_2 [13, 15] were synthesized. On the other hand, the synthesis of nanocrystalline ceramic materials imposes a challenge on the traditional solid state synthesis methods which fail to offer a sufficiently narrow size distribution and desired homogeneity at the nanometer level [17]. However, the hydrothermal synthesis method has an advantage for the production of highly crystalline and pure nanoparticles [18].

To the best of our knowledge, there is no report on the hydrothermal synthesis of lithium silicates, including lithium disilicate and nanoflower lithium metasilicate. Moreover, despite some significant experimental achievements, our knowledge on the electronic structure and optical properties of the crystalline lithium silicates is still rather limited. The electronic structure of the lithium metasilicate (Li_2SiO_3) and lithium disilicates ($Li_2Si_2O_5$) are previously calculated. However, the optical properties of these materials were not calculated.

Herein, we will report the synthesis of the highly crystalline and pure lithium metasilicate and lithium disilicate nanomaterials through a mild condition via hydrothermal method. Moreover, the powder X-Ray diffraction (PXRD) and scanning electron microscopy (SEM) analysis, as well as the UV-Vis and photoluminescence spectra of the synthesized materials will be discussed. Also, we will present the electronic and optical properties of the synthesized materials through the density functional theory calculations.

2. EXPERIMENTAL

2.1. Materials and methods

All chemicals were of analytical grade, synthesized from commercial sources and used without further purification. Phase identifications were performed on a powder Siemens D5000 X-Ray diffractometer using Cu-K_α radiation. The morphology of the synthesized materials was examined using Philips XL30 Scanning Electron Microscope. The absorption and photoluminescence spectra were recorded on a Jena Analytik Specord 40 and a Perkin Elmer LF-5 spectrometer, respectively.

2.1.1. Synthesis of lithium metasilicate

$LiNO_3$ (0.136 g, 2 mmole) was added to a solution of silicic acid (0.404 g, 4 mmole) in 30 mL of hot 0.01 M aqueous solution of NaOH while stirring. The resultant solution was stirred for further 15 min and then diluted to 60 mL. The obtained mixture was transferred to a 100 mL Teflon-lined autoclave and heated for 48, 72 or 96 h at 180°C. The resulting Li_2SiO_3 nanomaterials were filtered and dried at 110°C.

2.1.2. Synthesis of lithium disilicate

The preparation of $Li_2Si_2O_5$ was similar to that of Li_2SiO_3 except that the amounts of LiNO3 and silicic acid were changed (0.136 g, 2 mM and 0.606 g, 6mM, respectively). The obtained mixture was transferred to a 100 mL Teflon-lined autoclave and heated for 48, 72, 96 or 120 h at 180°C. The resulting compound Li2Si2O5 nanomaterials were filtered and dried at 110°C.

3. COMPUTATIONAL DETAIL

The electronic band structures along with density of states (DOS) of the compounds were calculated by density functional theory (DFT) using one of the three non-local gradient-corrected exchange-correlation functionals (GGA-PBE).

Calculations were performed using the CASTEP code [19, 20], which uses a plane wave basis set for

the valence electrons and norm-conserving pseudopotential (NCP) [21] for the core electrons.

The number of plane waves included in the basis was determined by a cutoff energy Ec of 500.0 eV. The summation over the Brillouin zone was carried out with a *k*-point sampling using a Monkhorst-Pack grid [22] with parameters of 5×5×5 and 4×5×2 for Li_2SiO_3 and $Li_2Si_2O_5$ respectively. Pseu-doatomic calculations were per-formed for Li-$2s^2$, Si-$3s^23p^2$, and O-$2s^22p^4$.

The parameters used in the calculations and conver-gence criteria were set by the default values of the CASTEP code, e.g., reciprocal space pseudopotentials representations, eigen-energy convergence tolerance of 1×10^{-6} eV, Gaussian smearing scheme with the smearing width of 0.1 eV, and Fermi energy convergence tolerance of 1×10^{-7} eV.

4. RESULTS AND DISCUSSION

4.1. PXRD analysis

Figure 1 in supplementary data represents the PXRD patterns of the obtained Li_2SiO_3 nanomate-rials after reaction time of 48, 72 and 96 h. The PXRD measurements confirm that when the Li:Si mole ratio in the reaction mixture is 1:2, a pure phase of the orthorhombic Li_2SiO_3 (space group of $Cmc2_1$ [23, 24]) is formed.

In contrast, as shown in Figure 2 in supplementary data, with the Li:Si mole ratio of 1:3 in the reaction mixture, a mixture of meta-stable $Li_2Si_2O_5$ (space group of *Pbcn* [25, 26]) and Li_2SiO_3 is obtained after 48 h. By increasing the reaction time to 72, 96 or 120 h, a pure high crystalline phase of meta-stable $Li_2Si_2O_5$ is obtained.

A stable form of this compound crystallizes in the space group of *Ccc*2 [27]. However, most papers refer to a monoclinic cell [28] despite noticing a discrepancy in diffraction peak intensities between experiment and calculation.

The monoclinic cell has a different symmetry but the same size as the *Ccc*2 stable form (β= 90°) [29].

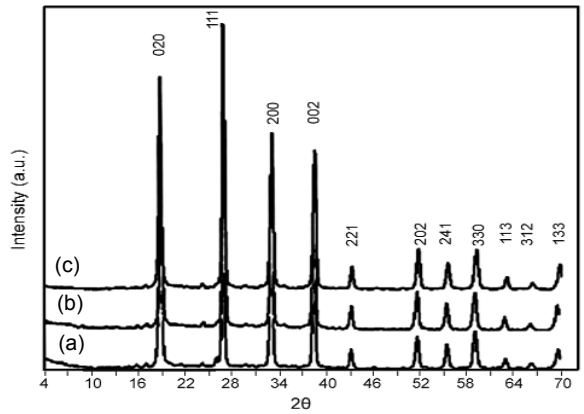

Figure 1: *PXRD patterns of the synthesized Li_2SiO_3 nanomaterials after (a) 48, (b) 72 and (c) 96 h at 180°C.*

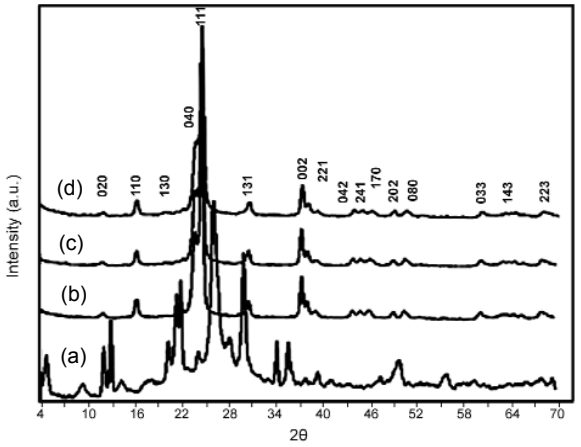

Figure 2: *PXRD patterns of the synthesized Li2Si2O5 nanomaterials after (a) 48, (b) 72, (c) 96 and (d) 120 h at 180°C.*

4.2. Microstructure analysis

The SEM images of the synthesized Li_2SiO_3 nanomaterials are given in Figure 3. With the reaction time of 48 h, ununiform sheet like nanoparticles of Li_2SiO_3 are obtained (Figure 3a). The thickness, widths and lengths of the resultant sheets are approximately 100 nm, 600 nm and 2 μm respectively. With increasing the reaction time to 72 h, the morphology of the obtained materials has been changed to the very compact sheets with heterogeneous morphology (Figure 3b). This is while, with the reaction time of 96 h, uniform flower like nanoparticles are obtained (Figure 3c).

Figure 4 represents the SEM images of the

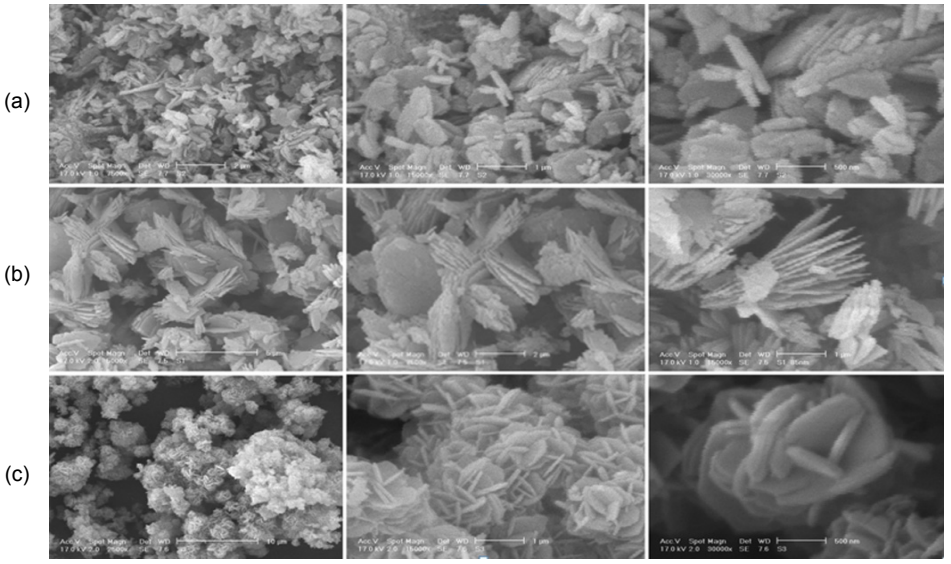

Figure 3: *The SEM images of the synthesized Li_2SiO_3 nanomaterials obtained after (a) 48, (b) 72 and (c) 96 h at 180°C.*

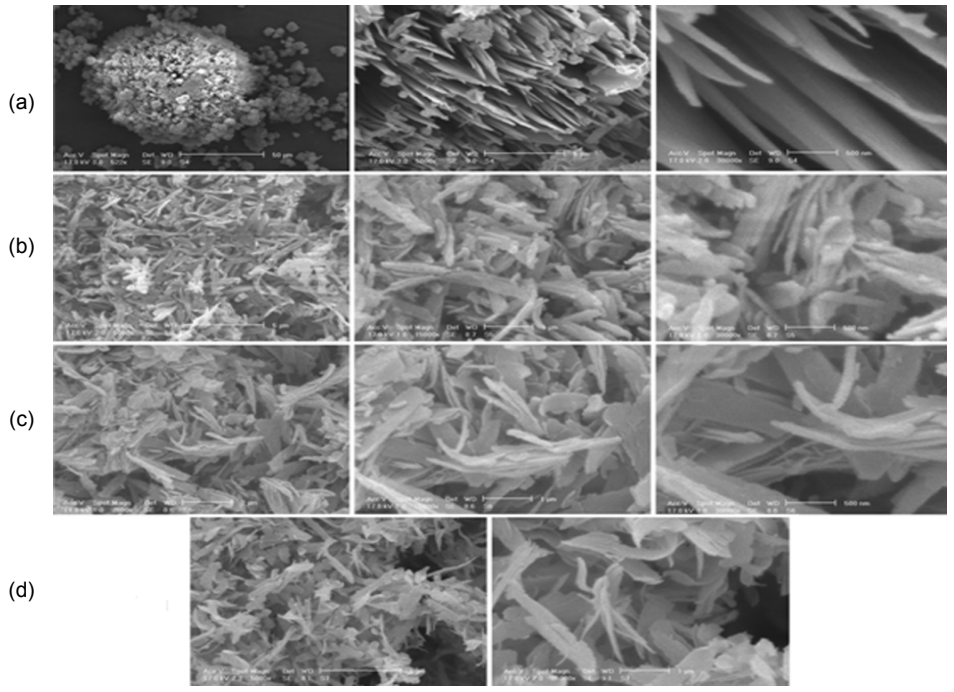

Figure 4: *The SEM images of the synthesized $Li_2Si_2O_5$ nanomaterials obtained after (a) 48, (b) 72, (c) 96 and (d) 120 h at 180°C.*

synthesized $Li_2Si_2O_5$ nanomaterials. After 48 h, the morphology of the obtained material is sponge like, consisting of sheet like and flower like nano-particles (Figure 4a). With increasing the reaction time to 72, 96 and 120 h, the morphology of the obtained materials has been changed to the rectangular sheets and high homogeny in the size is achieved.

4.3. Spectroscopic studies

The electronic absorption spectra and also the emission spectra of the synthesized Li_2SiO_3 and $Li_2Si_2O_5$ nanomaterials are given in Figure 5 and Figure 6 respectively. An intense absorption band at 276, 275 and 275 nm is observed in the electronic absorption spectra of the Li_2SiO_3 nanomaterials obtained after 48, 72 and 96 h at 180°C, respectively. A similar intense absorption band is observed at 272, 274 and 277 nm in the electronic absorption spectra of the $Li_2Si_2O_5$ nanomaterials obtained after 48, 72 and 96 h at 180°C, respectively.

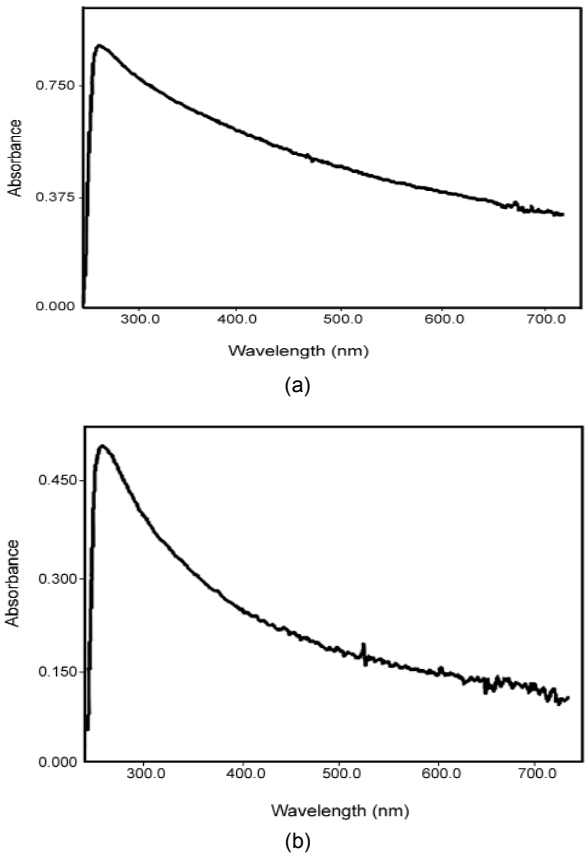

Figure 5: *The electronic absorption spectra of the synthesized Li_2SiO_3 (a) and $Li_2Si_2O_5$ (b) nanomaterials obtained after 96 h at 180°C.*

In the excitation spectrum of the synthesized Li_2SiO_3 and $Li_2Si_2O_5$ nanomaterials, a band is observed with maxima at 360 and 250 nm, respectively. Accordingly, in the emission spectrum of the synthesized Li_2SiO_3 nanomaterials, an intense peak appears at 410.03 nm. In comparison, an intense peak at 291.45 nm is observed in the emission spectrum of the synthesized $Li_2Si_2O_5$ nanomaterials. With increasing the reaction time, no shift is observed in the emission spectrum of obtained Li_2SiO_3 and $Li_2Si_2O_5$ nanomaterials. However, an increment in the band intensities in the emission spectra of both compounds is observed with increasing in the reaction time.

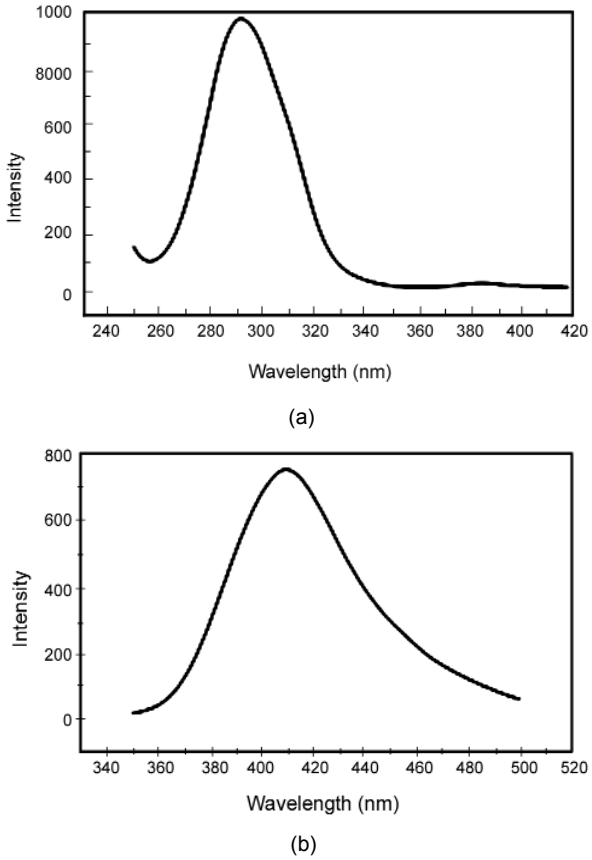

Figure 6: *The emission spectra of the synthesized Li_2SiO_3 (a) and $Li_2Si_2O_5$ (b) nanomaterials obtained after 96 h at 180°C.*

4.4. Structural optimization

The crystal structure and locations of the atoms of the Li_2SiO_3 [30] and $Li_2Si_2O_5$ [25] determined from X-ray diffraction data, are used as a starting point for total energy minimization. The experimental and calculated lattice parameters and also the calculated bond lengths and angles of the optimized structures are given in Tables 1 and 2 in supplementary data respectively. The optimized

Table 1: *The experimental and calculated lattice parameters of Li_2SiO_3 and $Li_2Si_2O_5$.*

species	Space group	experimental					calculated
Li_2SiO_3	$Cmc2_1$	a (Å) 9.392 [44]	9.3825 (a)	9.381 (b)	9.381 (c)		9.308913
		b (Å) 5.397	5.3985	5.398	5.403		5.363407
		c (Å) 4.660	4.6710	4.678	4.667		4.629192
$Li_2Si_2O_5$	Pbcn	a (Å) 5.683 [45]	5.814 (d)	5.815 (e)	5.835 (f)	5.825 (g)	5.663537
		b (Å) 4.784	4.793	4.749	4.806	4.796	4.755802
		c (Å) 14.648	14.630	14.630	14.540	14.560	14.457976

The cell parameters calculated from the PXRD patterns for the synthesized Li_2SiO_3 nanomaterials after (a) 48, (b) 72 and (c) 96 h and for the synthesized $Li_2Si_2O_5$ nanomaterials after (d) 48, (e) 72, (f) 96 and (g) 120 h at 180°C.

Table 2: *Selected bond lengths (Å) and angles (deg) of the optimized Li_2SiO_3 and $Li_2Si_2O_5$.*

Li_2SiO_3			
bond lengths:			
Si-O1	1.563	Si-O2	1.648
			1.645
Li-O1	1.928	Li-O2	2.183
	1.931		
	1.956		
bond angles:			
O1-Si-O1	116.599	O2-Si-O2	103.817
O1-Si-O2	108.733	Si-O2-Si	126.638
	109.098		
O1-Li-O1	106.274	O1-Li-O2	99.066
	106.523		109.960
	120.013		112.598
$Li_2Si_2O_5$			
bond lengths:			
Si-O1	1.579	Si-O2	1.552
Si-O3	1.614	Li-O2	1.924
	1.620		1.961
			2.016
Li-O3	2.094		
bond angles:			
O1-Si-O2	115.213	O1-Si-O3	106.818
			108.561
O2-Si-O3	109.296	O3-Si-O3	106.704
	109.882		
Si-O1-Si	160.668	Si-O3-Si	132.043
O2-Li-O2	97.448	O2-Li-O3	99.819
	106.068		105.092
	124.820		124.820

unit cells of the Li_2SiO_3 and $Li_2Si_2O_5$ are shown in Figure 7 and Figure 8 in supplementary data respectively. Optimization (relaxation) of the atomic positions and crystal cell parameters was performed befor the main calculations of the electronic characteristics, total electronic energy, band energy dispersion, density of electronic states and optical properties.

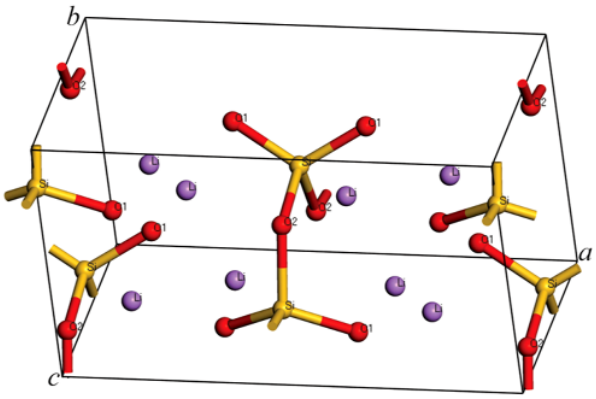

Figure 7

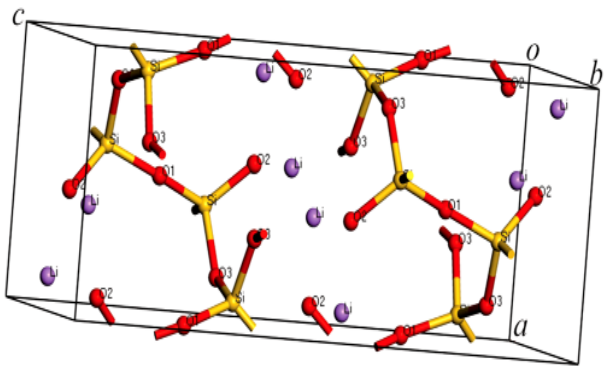

Figure 8

Figures 7, 8: *The optimized unit cells of the Li_2SiO_3 and $Li_2Si_2O_5$.*

4.5. Electronic structures

The calculated band structure of the compounds along high symmetry points of the first Brillouin zone is plotted in Figure 9, where the labeled k points are present as G (0.000, 0.000, 0.000), Z (0.000, 0.000, 0.500), T (-0.500, 0.500, 0.500), Y (-0.500, 0.500, 0.000), S (0.000, 0.500, 0.000), R (0.000, 0.500, 0.500) for Li_2SiO_3 and G (0.000, 0.000, 0.000), Z (0.000, 0.000, 0.500), T (-0.500, 0.000, 0.500), Y (-0.500, 0.000, 0.000), S (-0.500, 0.500, 0.000), X (0.000, 0.500, 0.000), U (0.000, 0.500, 0.500), R (-0.500, 0.500, 0.500) for $Li_2Si_2O_5$. It is found that the top of the valence bands (VBs) has a small dispersion, whereas the bottom of the conduction bands (CBs) has a big dispersion for both Li_2SiO_3 and $Li_2Si_2O_5$. The lowest energy (4.575 eV) of the conduction bands (CBs) of Li_2SiO_3 is localized at the G point, and the highest energy (0.00 eV) of VBs is localized at the Z point. In the case of the $Li_2Si_2O_5$, the lowest energy (4.776 eV) of the conduc-tion bands (CBs) is localized at the G point, and the highest energy (0.00 eV) of VBs is localized at the X point.

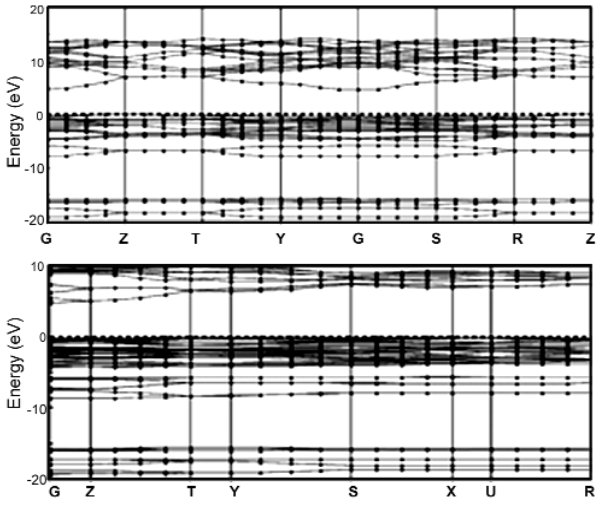

Figure 9: *Calculated band structure of Li_2SiO_3 (top) $Li_2Si_2O_5$ (bottom).*

As far as we know, the optical band gap of the bulk Li_2SiO_3 and $Li_2Si_2O_5$ has not been measured. It is well-known that both LDA and GGA density functional theory calculations systematically underestimate the band gap of insulators and semiconductors [1]. On the other hand, nano-materials, compared to the corresponding bulk materials, have wider band gap and therefore show a blue shift in the electronic absorption and photo-luminescence spectra [31]. In the orthogonalized linear combination of atomic orbital (OLCAO) calculations, the band gap of Li_2SiO_3 and $Li_2Si_2O_5$ was found to be 7.26 and 7.45 eV respectively [32, 33]. Also, a band gap of 5.7 eV [1] and 5.36 eV [34] for Li_2SiO_3 and 5.5 eV [1] for $Li_2Si_2O_5$ is

predicted by density functional theory (DFT) calculations using the generalized gradient approximation (GGA) within Perdew and Wang (PW91) scheme. However, according to our calculations, the values of the calculated band gap for Li_2SiO_3 and $Li_2Si_2O_5$ are 4.575 eV and 4.776 eV respectively, which are comparable with the experimental values (4.49 and 4.56 eV obtained for Li_2SiO_3 and $Li_2Si_2O_5$ nanomaterials obtained after 96h at 180°C), measured from the electronic absorption spectrum of the synthesized nanomaterials.

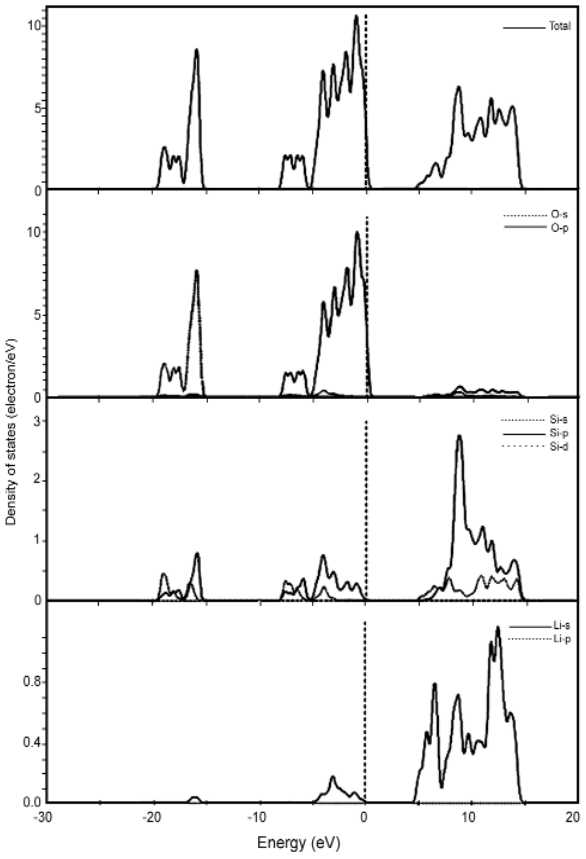

Figure 10: *Total and partial densities of states for Li_2SiO_3. The position of the Fermi level is set at 0.0 eV.*

The total density of states (TDOS) and partial densities of states (PDOS) for Li_2SiO_3 and $Li_2Si_2O_5$ are shown in Figure 10 and Figure 11 respectively. The VBs at -19.42 eV to -15.00 eV for Li_2SiO_3 and at -19.61 eV to -15.00 eV for $Li_2Si_2O_5$ has significant contributions from O-2s states; however, small contributions from Si-3s, 3p and Li-2s, O-2p states still can be observed at these energy intervals.

The most complex VBs are from -8.07 eV in Li_2SiO_3 and -8.84 eV in $Li_2Si_2O_5$ to the Fermi level (0.0 eV). According to the partial density of states, it is confirmed that the valence bands at these energy intervals are essentially formed by O-2p for both compounds, along with small admixture Li-2s, while the contributions from Si-3s, 3p states in $Li_2Si_2O_5$ are significant and cannot be neglected. Such characteristic indicates that covalent bonds could be formed among O-2p and Si-3p, 3s states in

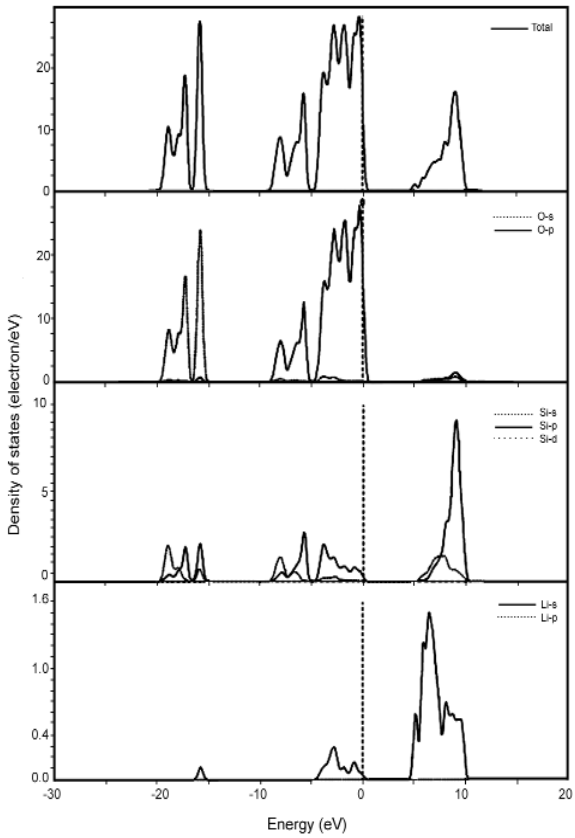

Figure 11: *Total and partial densities of states for $Li_2Si_2O_5$. The position of the Fermi level is set at 0.0 eV.*

$Li_2Si_2O_5$. However, in the case of Li_2SiO_3, these contributions are weaker. The valence bands at these energy ranges can be further divided into two parts. Such a splitting characteristic of valence bands reflects different bonding behaviors. The first parts located at -8.84 eV to -5.19 eV (for Li_2SiO_3)

and -8.07 eV to -4.62 eV (for $Li_2Si_2O_5$) is due to the bonding between Si-3s, 3p, Li-2s orbits and O-2p orbits, while the second part from -5.19 eV and -4.62 eV for Li_2SiO_3 and $Li_2Si_2O_5$ respectively to the Fermi level (0.0 eV) indicates the small interaction between Si-3p, Li-2s orbits and O-2p orbits. Analyzing the PDOS, also suggests ionic interactions between Si-2s, 2p orbits and O-2s, 2p orbits.

The conduction bands between 4.23 eV and 14.61 eV for Li_2SiO_3 come from Si-3s, 3p states, Li-2s states, and O-3s, 3p states. In comparison, the bands between 4.23 eV and 10.00 eV for $Li_2Si_2O_5$ come primarily from Si-3p states, with small contri bution from Si-3s states, Li-2s states O-2s, 2p states. The hybridization between Si-3s, 3p orbits and O-2s, 2p orbits at upper valence bands is the important structural character of the two compounds.

4.6. Optical properties

The optical properties can be gained from the complex dielectric function [33, 35]:

$$\varepsilon(\omega) = \varepsilon_1\omega) + i\,\varepsilon_2(\omega) \qquad (1)$$

which is mainly connected with the electronic structures and characterizes the linear response of the material to an electromagnetic radiation, and therefore governs the propagation behavior of radiation in a medium. The imaginary part of the dielectric function $\varepsilon_2(\omega)$ represents the optical absorption in the crystal, which can be calculated from the electronic structure through the joint density of states and the momentum matrix elements between the occupied and the unoccupied wave functions within the selection rules and is given by:

$$\varepsilon_2 = \frac{2e^2\pi}{\Omega\varepsilon_0}\sum_{k,v,c}\left|\left(\psi_k^c\left|\hat{u}\times r\right|\psi_k^v\right)\right|^2\delta\left(E_k^c - E_k^v - E\right) \qquad (2)$$

Where e is the electronic charge, and ψ_k^c and ψ_k^v are the conduction band (CB) and valence band (VB) wavefunctions at k, respectively.

The real part $\varepsilon_1(\omega)$ is evaluated from the imaginary part $\varepsilon_2(\omega)$ by the Kramers-Kronig transformation. The other optical constants such as the refractive index $n(\omega)$, extinction coefficient $k(\omega)$, optical reflectivity $R(\omega)$ absorption coefficient $\alpha(\omega)$, energy-loss spectrum $L(\omega)$ and the complex conductivity function $\sigma(\omega)$ can be computed from the complex dielectric function $\varepsilon_1(\omega)$, through the following relations [35, 36]:

$$n(\omega) = \sqrt{\left|\,\varepsilon(\omega)\,\right| + \varepsilon_1(\omega)}\Big/2 \qquad (3)$$

$$k(\omega) = \sqrt{\left|\,\varepsilon(\omega)\,\right| - \varepsilon_1(\omega)}\Big/2 \qquad (4)$$

$$R(\omega) = \frac{(n-1)^2 + k^2}{(n+1)^2 + k^2} \qquad (5)$$

$$\alpha(\omega) = 2k\omega\Big/c \qquad (6)$$

$$L(\omega) = \mathrm{Im}\left(\frac{-1}{\varepsilon(\omega)}\right) = \frac{\varepsilon_2(\omega)}{\varepsilon_1^2(\omega) + \varepsilon_2^2(\omega)} \qquad (7)$$

$$\sigma(\omega) = \sigma^{1(\omega)} + i\sigma^{2(\omega)} = -i\frac{\omega}{4\pi}\left[\varepsilon(\omega) - 1\right] \qquad (8)$$

The dielectric functions of Li_2SiO_3 and $Li_2Si_2O_5$ were calculated based on the electronic structure. The $\varepsilon_1(\omega)$ and $\varepsilon_2(\omega)$ as a function of the photon energy are shown in Figure 12 for Li_2SiO_3 and $Li_2Si_2O_5$.

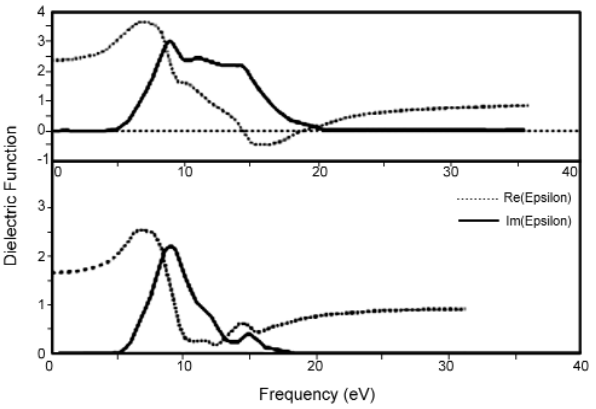

Figure 12: *Dielectric functions of Li_2SiO_3 (top) $Li_2Si_2O_5$ (bottom).*

The imaginary part of $\varepsilon(\omega)$ in Li_2SiO_3 has three intense bands located at 9.02 eV, 11.11 eV, 14.35 eV. The first Peak corresponds mainly to the transition from O-2p states (VBs) to the empty Li-2s and Si-3s states (CBs) above the Fermi level. The second and third peaks are mainly due to the transitions from O-2p states (VBs) to the Si-3p and Li-2s states (CBs) above the Fermi level. In contrast, $Li_2Si_2O_5$ has a prominent absorption peak, located at the photon energies of 9 eV and two weaker bands located at 11.74 eV and 15 eV. The main peak at the 9 eV is due to strong interband transitions between the O-2p states (VBs) and Si-3p empty states (CBs). It is noted that a peak in $\varepsilon_2(\omega)$ does not correspond to a single interband transition since many direct or indirect transitions may be found in the band structure with an energy corresponding to the same peak [37]. The peak amplitudes of Li_2SiO_3 are larger than those of the $Li_2Si_2O_5$ crystals, due to the fact that the band structures for the two compounds are not similar.

For the real part $\varepsilon_1(\omega)$ of the dielectric function $\varepsilon(\omega)$, the most important quantity is the zero fre-quency limit $\varepsilon_1(0)$, which is the electronic part of the static dielectric constant and depends strongly on the band gap. A smaller energy gap yields a larger $\varepsilon_1(0)$ value. This could be ex-plained on the basis of the Penn model [38]:

$$\varepsilon_1(0) \approx 1 + (h\omega_p / E_g)^2 \quad (9)$$

The energy gap (E_g) could be determined from this expression by using the values of $\varepsilon_1(0)$ and the plasma energy $h\omega_p$. The calculated and experimental E_g and also the calculated static dielectric constants $\varepsilon_1(0)$ of Li_2SiO_3 and $Li_2Si_2O_5$ are listed in Table 3.

The experimental E_g values calculated from the UV-Vis spectra for the synthesized Li_2SiO_3 and $Li_2Si_2O_5$ nanomaterials after (a) 48, (b) 72 and (c) 96 h at 180°C. The calculated results on the absorption, reflectivity and energy-loss spectra by norm-conserving pseudopotentials were shown in Figures 13-15.

According to the absorption spectra, the absorption edges are located at 9.11, 11.85 and 14.70 eV for Lithium metasilicate and at 8.2, 11.60 and 15 eV for Lithium disilicate. The absorption coefficients decrease rapidly in the low-energy region, which is the representative character of the semiconductors and insulators.

The calculated reflectivity for lithium metasilicate at 0-5 eV is lower than 10% and amaximum value of roughly 35.0% is calculated at about 17.53 eV. In comparison, the reflectivity for lithium disilicate at 0-5 eV is calculated to be lower than 2%. The calculated reflectivity spectrum of lithium disilicate shows a maximum value of about 15% at 9.9 eV. According to the absorption and reflectivity spectra, it is concluded that lithium metasilicate and lithium disilicate are transmitting for frequencies < 4.00 eV.

The energy-loss spectrum describes the energy-loss of a fast electron traversing in the material [39].

Table 3: *Theoretical and experimental energy gaps (E_g) and the calculated average static dielectric constant of Li_2SiO_3 and $Li_2Si_2O_5$.*

	Li_2SiO_3		$Li_2Si_2O_5$	
	Calc.	Exp.	Calc.	Exp.
pseudopotentials	norm-conserving	-	norm-conserving	-
E_g (eV)	4.575	4.49 (a) 4.51 (b) 4.51 (c)	4.776	4.56 (a) 4.53 (b) 4.48 (c)
$\varepsilon_1(0)$	2.39	-	1.70	-

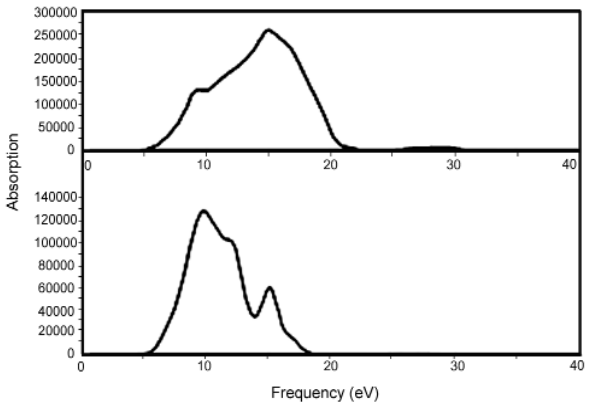

Figure 13: *Calculated absorption spectra of Li_2SiO_3 (top) $Li_2Si_2O_5$ (bottom).*

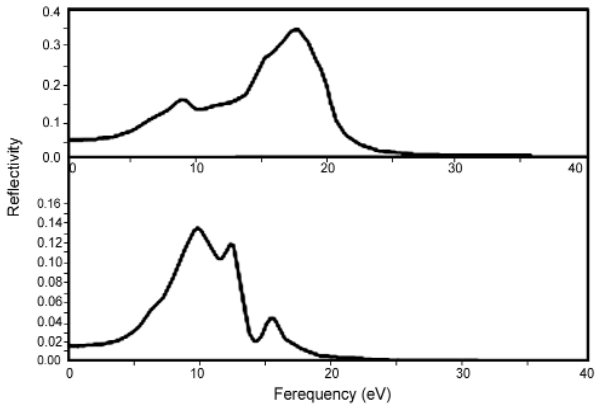

Figure 14: *Calculated reflectivity of Li_2SiO_3 (top) $Li_2Si_2O_5$ (bottom).*

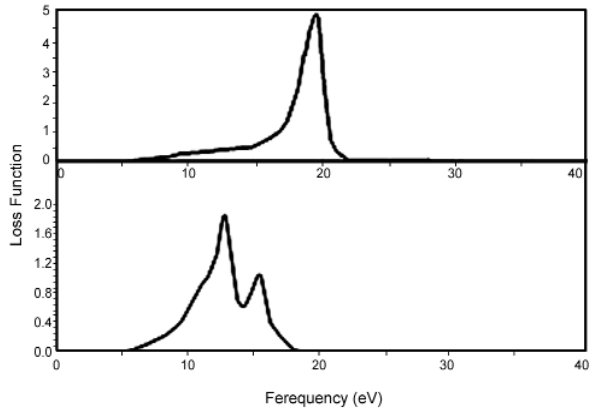

Figure 15: *Calculated Energy loss function for Li_2SiO_3 (top) $Li_2Si_2O_5$ (bottom).*

The main peak is generally defined as the bulk plasma frequency [40]. At energies smaller than 5.0 eV, no distinct peak is calculated due to the fact that $\varepsilon_2(\omega)$ is still large at these energy values. The main peaks of energy-loss spectra, as shown in Figure 15, are calculated at about 12.82 eV and 15.55 eV for lithium disilicate and 19.5 eV for lithium metasilicate. Such calcula-tions may stimulate the experimental investigations.

5. CONCLUSIONS

This study describes the hydrothermal synthesis of highly crystalline and pure lithium metasilicate and lithium disilicate nanoparticles. The PXRD patterns indicate that the pure lithium metasilicate and lithium disilicate well crystallized under hydro-thermal condition.

SEM images show the reaction time effect on the morphology and homogeneity of the synthesized materials. The intensity of the bands in the emission spectra increases with increasing reaction time in both lithium metasilicate and lithium disilicate.

The electronic band structure along with density of states (DOS) calculated by the DFT method indicates that Li_2SiO_3 and $Li_2Si_2O_5$ have an indirect energy band gap of about 4.575 eV and 4.776 eV respectively. The hybridized interactions between Si-3s, 3p orbits and O-2p orbits are revealed as the important structural characteristics of the two compounds, which leads to large band gaps.

The optical properties, including the dielectric function, absorption coefficient, reflectivity and energy-loss spectra, also have been calculated by DFT methods.

According to the calculated absorption and reflectivity spectra, Li_2SiO_3 and $Li_2Si_2O_5$ are theoretically transmitting for frequencies < 4.00 eV.

Therefore, Li_2SiO_3 and $Li_2Si_2O_5$ are the excellent visible and IR transparent mate-rials, which have been experimentally proved. Furthermore, for both compounds, the imaginary part $\varepsilon_2(\omega)$ of the dielectric function $\varepsilon(\omega)$ has been discussed in detail according to the band structure.

It is found that the peak intensities in Li_2SiO_3 are obviously enhanced compared to that in $Li_2Si_2O_5$.

ACKNOWLEDGEMENTS

We are grateful to the University of Tabriz Research Council for the financial support of this research.

REFERENCES

1. Du J., Corrales L.R., *J. Phys. Chem. B.*, **110**(2006), 22346.
2. Beall G.H., *Annu. Rev. Mater. Sci.*, **22**(1992), 91.
3. Vincent C.A., *Solid State Ionics*, **134**(2000), 159.
4. Lu C.H., Cheng L.W., *J. Mater. Chem.*, **10**(2000), 1403.
5. Broussely M., Perton F., Biensan P., Bodet J.M., Labat J., Lecerf A., Delmas C., Rougier A., Peres J.P., *J. Power Sources.*, **54**(1995), 109.
6. Subramanian V., Chen C.L., Chou H.S., Fey G.T.K., *J. Mater. Chem.*, **11**(2001), 3348.
7. Vinod M.P., Bahnemann D., *J. Solid State Electrochem.*, **6**(2002), 498.
8. Zhang B., Easteal A.J., *J. Mater. Sci.*, **43**(2008), 5139.
9. Cruz D., Bulbulian S., Lima E., Pfeiffer H., *J. Solid State Chem.*, **179**(2006), 909.
10. Nakazawa T., Yokoyama K., Noda K., *J. Nucl. Mater.*, **258**(1998), 571.
11. Munakata K., Yokoyama Y., *J. Nucl. Sci. Technol.*, **38**(2001), 915.
12. Khomane R.B., Sharma B.K., Saha S., Kulkarni B.D., *Chem. Eng. Sci.*, **61**(2006), 3414.
13. Pfeiffer H., Bosch P., Bulbulian S., *J. Nucl. Mater.*, **257**(1998), 309.
14. Van der Laan J.G., Kawamura H., Roux N., Yamaki D., *J. Nucl. Mater.*, **283**(2000), 99.
15. Cruz D., Bulbulian S., *J. Am. Ceram. Soc.*, **88**(2005), 1720.
16. Ortiz-Landeros J., Contreras-Garcia C.E., Gomez-Yanez Pfeiffer H., *J. solid State Chem.*, **184**(2011), 1304.
17. Khomane R.B., Sharma B.K., Saha S., Kulkarni B.D., *Chem. Eng. Sci.*, **61**(2006), 3415.
18. Simoes A.Z., Moura F., Onofre T.B., Ramirez M.A., Varela J.A., Longo E., *J. Alloy. Compound*, **508**(2010), 620.
19. S.J. Clark, M.D. Segall, C.J. Pickard, P.J. Hasnip, M.J. Probert, K. Refson, M.C. Payne, 2009. *Materials Studio CASTEP*, version 5.0, Accelrys: San Diego, CA.
20. Clark S.J., Segall M.D., Pickard C.J., Hasnip P.J., Probert M.J., Refson K., Payne M.C., *Z. Kristallogr.*, **220**(2005), 567.
21. Hamann D.R., Schluter M., Chiang C., *Phys. Rev. Lett.*, **43**(1979), 1494.
22. Monkhorst H.J., Furthmuller J., *Phys. Rev. B.*, **13**(1976), 5188.
23. Kalinkin A.M., Kalinkina E.V., Zalkind O.A., Makarova T.I., *Colloid J.*, **70**(2008), 42.
24. Beneke K., Thiesen P., Lagaly G., *Inorg. Chem.*, **34**(1995), 900.
25. Smith R.I., Howie R.A., West A.R., Pina A.A., Villafuerte-Castrejon M.E., *Acta Crystallogr., Sect. C: Cryst. Struct. Commun.*, **46**(1990), 363.
26. Smith R.I., West A.R., Abrahams I., Bruce P.G., *Powd. Diffract*, **5**(1990), 137.
27. Liebau F., *Acta Crystallogr.*, **14**(1961) 389
28. De jong B.H.W.S., Supér H.T.J., Spek A.L., Veldman N., Nachtegaal G., Fischer J.C., *Acta Crystallogr., Sect. B: Struct. Sci.*, **54**(1998), 568.
29. Paszkowicz W., Wolska A., Klepka M.T., All S.A.E., Eldin F.M.E., *Acta Phys. Pol., A.*, **117**(2010), 315.
30. Hesse K.F., *Acta Crystallogr., Sect. B: Struct. Sci.*, **33**(1977), 901.
31. D. Vollath, 2008. *Nanomaterials: An Introduction to Synthesis, Properties and Applica-tions*, Wiley, Weinheim.
32. H.E. Schaefer, 2010. Nanoscience: *The Science of the Small in Physics, Engineering, Chemistry, Biology and Medicine*, Springer, Berlin.
33. Ching W.Y., Li Y.P., Veal B.W., Lam D., *J. Phys. Rev. B.*, **32**(1985), 1203.
34. Tang T., Luo D.L., *J. At. Mol. Sci.*, **1**(2010), 185.
35. R.C. Fang, 2003. *Solid State Spectroscopy*,

Chinese Science Technology University Press, Hefei.
36. Y. Zhang, W.M. Shen, 2005. *Basic of Solid Electronics*, Zhe Jiang University Press, Hangzhou.
37. De Almeida J.S., Ahuja R., *Appl. Phys. Lett.*, **89**(2006), 061913.
38. Penn D.R., *Phys. Rev.*, **128**(1962), 2093.
39. Bouhemadou A., Khenata R., *Comput. Mater. Sci.*, **39**(2007), 803.
40. Saniz R., Ye L.H., Shishidou T., Freeman A.J., *Phys. Rev. B.*, **74**(2006), 014209.